The Cryosphere Discuss., 8, 3733–3783, 2014
www.the-cryosphere-discuss.net/8/3733/2014/
doi:10.5194/tcd-8-3733-2014

The Cryosphere Discussions
Open Access

Assessing spatio-temporal variability and trends (2000–2013) of modelled and measured Greenland ice sheet albedo

P. M. Alexander[1,2], M. Tedesco[2,1], X. Fettweis[3], R. S. W. van de Wal[4], C. J. P. P. Smeets[4], and M. R. van den Broeke[4]

[1]Graduate Center of the City University of New York, 365 5th Ave., New York, NY, 10016, USA
[2]City College of New York, City University of New York, 160 Convent Ave., New York, NY, 10031, USA
[3]Department of Geography, Université de Liège, Place du 20-Août, 7, 4000 Liège, Belgium
[4]Institute for Marine and Atmospheric research Utrecht, Utrecht University, Princetonplein 5, 3584 CC Utrecht, the Netherlands

Received: 28 April 2014 – Accepted: 18 June 2014 – Published: 15 July 2014

Correspondence to: P. M. Alexander (palexander@gc.cuny.edu)

Published by Copernicus Publications on behalf of the European Geosciences Union.

Abstract

Accurate measurements and simulations of Greenland Ice Sheet (GrIS) surface albedo are essential, given the crucial role of surface albedo in modulating the amount of absorbed solar radiation and meltwater production. In this study, we assess the spatiotemporal variability of GrIS albedo (during June, July, and August) for the period 2000–2013. We use two remote sensing products derived from data collected by the Moderate Resolution Imaging Spectroradiometer (MODIS), as well as outputs from the Modèle Atmosphérique Régionale (MAR) regional climate model (RCM) and data from in situ automatic weather stations. Our results point to an overall consistency in spatiotemporal variability between remote sensing and RCM albedo, but reveal a difference in mean albedo of up to ∼ 0.08 between the two remote sensing products north of 70° N. At low elevations, albedo values simulated by the RCM are positively biased with respect to remote sensing products and in situ measurements by up to ∼ 0.1 and exhibit low variability compared with observations. We infer that these differences are the result of a positive bias in simulated bare-ice albedo. MODIS albedo, RCM outputs and in situ observations consistently point to a decrease in albedo of −0.03 to −0.06 per decade over the period 2003–2013 for the GrIS ablation zone (where there is a net loss of mass at the GrIS surface). Nevertheless, satellite products show a decline in albedo of −0.03 to −0.04 per decade for regions within the accumulation zone (where there is a net gain of mass at the surface) that is not confirmed by either the model or in situ observations.

1 Introduction

Over the past decade, the Greenland Ice Sheet (GrIS) has simultaneously experienced accelerating mass loss (van den Broeke et al., 2009; Rignot et al., 2011) and records for the extent and duration of melting (Tedesco et al., 2008, 2011, 2013; Nghiem et al., 2012). Besides the direct relationship between temperature and melt-

TCD
8, 3733–3783, 2014

ing, increased melt over Greenland has been associated with an amplifying ice-albedo feedback: increased melting and bare ice exposure reduce surface albedo, thereby increasing the amount of absorbed solar radiation and, in turn, further accelerating melting (Box et al., 2012; Tedesco et al., 2011). Recent studies (van den Broeke et al., 2011; Vernon et al., 2013) also indicate that albedo plays an essential role in the GrIS surface energy balance, and consequently, the surface mass balance (SMB) of those regions where considerable melting occurs. Because of the impact of albedo on the surface energy balance, it is crucial to assess the performance of models that simulate albedo over the GrIS and the quality of albedo estimates from remote sensing or in situ observations. These assessments are pivotal for improving our understanding of the physical processes leading to record mass loss, and for improving projections for the next decades.

Several studies that have investigated GrIS albedo trends and variability have primarily relied on satellite measurements, particularly those collected by the Moderate Resolution Imaging Spectroradiometer (MODIS) (e.g. Stroeve et al., 2005, 2006, 2013; Box et al., 2012). Remote sensing measurements can capture changes at large spatial scales and for long periods, continuously (with the exception of cases when the surface is obscured by clouds). Previous studies have found MODIS albedo products to agree reasonably well with in situ data, especially with regards to capturing the seasonal albedo cycle and mean seasonal values in regions where variability is small (Stroeve et al., 2005, 2006, 2013), but lower accuracy at high solar zenith angles has been identified (Stroeve et al., 2005, 2006; Wang and Zender, 2009), limiting the periods and locations for which these data can be used. On the other hand, we note that regional climate models (RCMs) are an important tool for estimating both current and future changes in the GrIS SMB (Box and Rinke, 2002; Box et al., 2006; Ettema et al., 2009; Fettweis et al., 2007, 2011; Rae et al., 2012; Tedesco and Fettweis, 2012), with the surface albedo schemes (and in particular the bare ice albedo parameterizations) employed by these models having a substantial impact on their simulation of the SMB (Rae et al., 2012; van Angelen et al., 2012; Lefebre et al., 2005; Franco et al., 2012).

TCD
8, 3733–3783, 2014

In this paper, we report the results of an assessment of GrIS albedo spatio-temporal variability and trends through the analysis of different remote sensing products, in situ measurements and the outputs of two different versions of an RCM, featuring different albedo schemes. To our knowledge, this is the first-time that a multi-tool integrated assessment of albedo over Greenland is presented. We introduce the MAR model, the MODIS products and the GrIS in situ data in Sect. 2. In Sect. 3, we compare spatio-temporal variability of the two MODIS satellite products, in situ data, and MAR outputs, and discuss these results in Sect. 4. Conclusions are presented in Sect. 5.

2 Data and methods

2.1 The MAR model

The Modèle Atmosphérique Régionale (Gallée and Schayes, 1994; Gallée, 1997; Lefebre et al., 2003), abbreviated MAR, is a coupled land-atmosphere regional climate model featuring the atmospheric model described by Gallée and Shayes (1994) and the Soil Ice Snow Vegetation Atmosphere Transfer scheme (SISVAT) surface model. SISVAT incorporates the multilayer snow model *Crocus* (Brun et al., 1992), which simulates fluxes of mass and energy between snow layers, and reproduces snow grain properties and their effect on surface albedo. The model setup used here is described in detail by Fettweis (2007). We use a recent version of MAR (v3.2), which features changes to the albedo scheme relative to previous versions (v1 and v2), detailed in Sect. 2.2. MAR has been run at a 25 km horizontal resolution for the period 1958–present. The model is forced at its lateral boundaries and ocean surface and initialized with 6 hourly reanalysis data from the European Centre for Medium-Range Weather Forecasts (ECMWF), using the ERA-40 reanalysis for the period 1958–1978 and the ERA-Interim reanalysis for the period 1979–present. Here we focus on the 2000–2013 period for comparison with satellite data. The MAR v3.2 ice sheet mask (which gives the fraction covered by ice for each grid box) and surface elevation are defined using

TCD
8, 3733–3783, 2014

the Greenland digital elevation model of Bamber et al. (2013). Originally, MAR v2.0 used the elevation model of Bamber et al. (2001), and the land surface classification mask from Jason Box (sites.google.com/site/jboxgreenland/datasets).

In MAR v3.2, in contrast with MAR v2.0 (used by Fettweis et al., 2013a, b), sub-grid scale parameterizations make it possible to have fractions of different land cover types within a single grid box. Quantities are computed for the sectors within each grid box and a weighted average of these quantities is used to represent the average value for a grid box. Here, we conduct comparisons with satellite data only for pixels classified as 100 % covered by ice (to avoid including satellite pixels over tundra in the comparison). For some in situ stations along the edges of the ice sheet, we have compared in situ and satellite data with MAR estimates of albedo within the "ice-covered" sector of the encompassing MAR grid box.

For the reader's convenience, we show the mean September 2000–August 2013 SMB from MAR v3.2 in Fig. 1, along with the equilibrium line dividing positive and negative SMB, together with the locations of the weather stations used in this study. In this study, areas below the mean 2000–2013 equilibrium line as defined by MAR are collectively referred to as the "ablation zone", while areas above this line are referred to as the "accumulation zone".

2.2 The MAR albedo scheme

The basis for the MAR albedo scheme is described in detail by Brun et al. (1992) and Lefebre et al. (2003). MAR snow albedo depends on the optical diameter of snow grains, which is in turn a function of other snow grain properties. Larger, more spherical, less dendritic particles result in a higher optical diameter, and vice versa. In the model, the sphericity, dendricity, and size of snow grains are a function of snowpack temperature, temperature gradient, and liquid water content. MAR albedo (α) is a function of snow grain optical diameter (d) in meters for three spectral bands for visible,

TCD
8, 3733–3783, 2014

near infrared and far infrared radiation:

$$\text{Band 1 (0.3–0.8 µm)}: \ \alpha_1 = \max(0.94, 0.96 - 1.58\sqrt{d}) \quad (1)$$

$$\text{Band 2 (0.8–1.5 µm)}: \ \alpha_2 = 0.95 - 15.4\sqrt{d} \quad (2)$$

$$\text{Band 3 (1.5–2.8 µm)}: \ \alpha_3 = 364 \cdot \min(d, 0.0023) - 32.31\sqrt{d} + 0.88 \quad (3)$$

where α_1, α_2, and α_3 are wavelength dependent albedo values over the three spectral bands. The integrated snow albedo (α_S) for the range 0.3 to 2.8 µm is a weighted average of albedo over these bands based on solar irradiance fractions:

$$\alpha_S = 0.580\alpha_1 + 0.320\alpha_2 + 0.1\alpha_3 \quad (4)$$

The minimum albedo of snow is set to 0.65. In MAR v2.0, bare ice albedo was simply assigned a fixed value of 0.45. In MAR v3.2 (the version primarily used here), bare ice albedo is a function of accumulated surface water following the parameterizations of Lefebre et al. (2003), described below. In the case of bare ice (which occurs in MAR when the surface snow density is greater than 920 kg m^{-3}) ice albedo (α_I) is given by:

$$\alpha_I = \alpha_{I,\min} + (\alpha_{I,\max} - \alpha_{I,\min}) e^{-\left(\frac{M_{SW}(t)}{K}\right)} \quad (5)$$

Where $\alpha_{I,\min}$ and $\alpha_{I,\max}$ are the minimum and maximum bare ice albedo (set to 0.45 and 0.55 respectively for MAR v3.2), K is a scale factor (set to 200 kg m^{-2}), and $M_{SW}(t)$ is the time-dependent accumulated amount of excessive surface meltwater before runoff (in kg m^{-2}). According to the parameterization of Zuo and Oerlemans (1996), there is delay in MAR v3.2 between the production of meltwater and evacuation towards the oceans (Lefebre et al., 2003), in order to account for the reduction of bare ice albedo due to the presence of surface water. The ice surface albedo (α_I) will therefore be lower if the melt rate is higher, asymptotically approaching the minimum bare ice albedo.

Additionally, to ensure temporal continuity in simulated albedo, values of albedo between the maximum bare ice and minimum snow albedo (0.55 and 0.65 respectively for

TCD
8, 3733–3783, 2014

MAR v3.2) are possible when the surface (or near-surface) snow density lies between 830 and 920 kg m^{-3}. In this case (which corresponds to the presence of firn), albedo (α_I) is a function of density as follows (Lefebre et al., 2003):

$$\alpha_I = \alpha_{I,max} + (\alpha_{S,min} - \alpha_{I,max}) \left(\frac{\rho_I - 920\,kg\,m^{-3}}{\rho_C - 920\,kg\,m^{-3}} \right) \quad (6)$$

where $\alpha_{S,min}$ is the minimum albedo of snow (0.65), ρ_I is the density of the upper firn layer, and ρ_C is the density at which pores within firn close off (830 kg m^{-3}). In cases where there is a snowpack with a thickness of < 10 cm overlaying ice or firn (with a density greater than 830 kg m^{-3}), excluding the case of ice lenses, albedo is interpolated between the ice albedo and the surface snow albedo as a linear function of snowpack thickness, to produce an "integrated" surface albedo of snow, ice and water (α_{SI}):

$$\alpha_{SI} = \alpha_I + \alpha_S(H_S/0.1) \quad (7)$$

where H_S is the snowpack height in meters. In cases where a snowpack thicker than 0.1 m lies above ice, or there is bare ice at the surface, α_{SI} is simply set equal to the snow albedo (α_S), or bare-ice albedo (α_I), respectively.

Snow albedo is generally higher during cloudy conditions due to the masking of a portion of the incoming solar spectrum by clouds (Greuell and Konzelman, 1994). MAR accounts for this factor by applying a correction to the integrated surface albedo (α_{SI}) as a function of cloud fraction, following Greuell and Konzelman (1994):

$$\alpha_{CL} = \alpha_{SI} + 0.05(n - 0.5) \quad (8)$$

where n is the cloud fraction computed by MAR, and α_{CL} is the cloud-corrected albedo. Satellite data can only provide cloud-free measurements, and therefore we re-correct MAR surface albedo to produce estimates of cloud-free surface albedo. We use this

TCD
8, 3733–3783, 2014

particular technique rather than excluding "cloudy" data from MAR because MAR does not necessarily replicate the actual cloud fraction observed by MODIS. The correction factor applied here reverses the correction applied in MAR, then corrects albedo for the case where there is a cloud fraction of 0:

$$\alpha_{\text{MAR,clear-sky}} = \alpha_{\text{MAR,daily}} - 0.05(n_{\text{MAR,daily}} - 0.5) - 0.025 \quad (9)$$

In this case $\alpha_{\text{MAR,daily}}$ is the daily mean MAR albedo, $n_{\text{MAR,daily}}$ is the daily mean cloud fraction from MAR, and $\alpha_{\text{MAR,clear-sky}}$ is the daily mean clear-sky albedo. All following analyses with MAR data are conducted using $\alpha_{\text{MAR,clear-sky}}$.

2.3 Satellite-derived albedo

We use the daily MODIS albedo product (MOD10A1, Version-5) distributed by the National Snow and Ice Data Center (Hall et al., 2012; available at http://nsidc.org/data/mod10a1.html) and the 16 day (MCD43A3, Version-5) product from Boston University (Schaaf et al., 2002; available at: https://lpdaac.usgs.gov/).

The MOD10A1 Version-5 product contains daily albedo (0.3–3 µm) based on the "best" daily MODIS observation, defined as the observation that covers the greatest percentage of a grid cell. Corrections are also applied to account for anisotropic scattering, for the influence of the atmosphere on surface albedo, and for the limited spectral range of MODIS bands (Klein and Stroeve, 2002; Stroeve et al., 2006). Here we use MODIS data from the TERRA satellite, as MODIS data from the AQUA satellite are less reliable due to an instrument failure in the near infrared band (Stroeve et al., 2006; Box et al., 2012).

The MCD43A3 Version-5 product makes use of all atmospherically-corrected MODIS reflectance measurements over 16 day periods to provide an integrated albedo measurement every 8 days. A semi-empirical bidirectional reflectance function (BRDF) model is used to compute bi-hemispherical reflectance as a function of these reflectance measurements (Schaaf et al., 2002). The MCD43A3 product contains, in

TCD
8, 3733–3783, 2014

addition to albedo values for each MODIS instrument band, "shortwave" albedo values calculated over a wavelength interval of 0.3–5.0 µm and "visible" albedo values for the 0.3–0.7 µm interval, calculated using the BRDF parameters. Here we primarily make use of "shortwave" MCD43A3 albedo, as its wavelength interval is consistent with those of MAR and MOD10A1, but briefly consider "visible" albedo as well. The MCD43A3 product provides, over each wavelength interval, an integrated diffuse White Sky Albedo (WSA) and a direct Black Sky Albedo (BSA) for a specific viewing geometry (from above when the local solar zenith angle is at a maximum). A linear combination of WSA and BSA can be used to compute the true "blue-sky albedo". Stroeve et al. (2005) suggest that there is little difference between BSA and WSA for typical summer noontime solar zenith angles over Greenland. Simulation of blue-sky albedo requires models or observations of aerosol optical depth (e.g. Stroeve et al., 2013) that are not available for this study and therefore, the following results consider BSA only.

Both MODIS products provide quality flags indicating "good quality" vs. "other quality" data. In the case of MCD43A3, "other quality" data are produced using a "backup" algorithm. When few observations are available, the backup algorithm is used to scale an archetypal BRDF function that is based on past observations (Schaaf et al., 2002). In order to understand the influence of data quality on our results, we present results for both "all quality" as well as "good quality" data. For our purposes, MODIS albedo products are re-gridded to the MAR 25 km resolution grid from the original 463 m spatial resolution at which they are distributed. Re-gridded values contain the median value of all the MODIS values falling within a MAR grid box. As mentioned, we restrict our analysis to the GrIS, excluding areas where the MAR sub-grid level ice cover percentage is less than 100 %, except for comparison with in situ data, in which case we use data from individual MODIS pixels, in situ measurements, and MAR ice-covered sector data.

TCD
8, 3733–3783, 2014

2.4 Weather station data

We use Automatic Weather Station (AWS) data from two sources, the Greenland Climate Network (GC-Net, Steffen et al., 1996) and the Kangerlussuaq Transect (K-Transect, van de Wal et al., 2005). The locations of the weather stations are shown in Fig. 1, and a list of the weather stations used and their period of coverage is provided in Table 1. We use all available GC-Net and K-transect June-July-August (JJA) data within the period 2000–2012 for comparison with MODIS and MAR albedo. (GC-Net data for the summer of 2013 were not yet available when data analysis for this study was conducted.) We follow a procedure similar to that employed by Stroeve et al. (2005) to generate albedo timeseries' from GC-Net and K-Transect data. Mean daily albedo was computed as the sum of daily incident shortwave (SW) radiation divided by the sum of daily outgoing SW radiative flux. Instances where hourly upward SW radiative flux exceeds downward SW radiative flux were excluded. Upward and downward hourly radiative fluxes were excluded when downward fluxes were smaller than $250\,\mathrm{W\,m^{-2}}$ to reduce the impact of relative errors on measured albedo, especially during cases of low incident radiation. (We investigated the sensitivity of our results to this threshold, and did not find a considerable effect on the results.) Data from several locations and time periods were excluded from this analysis. These stations are included in Table 1. In particular, measured albedo at Swiss Camp for the year 2012 appeared to be unrealistically high relative to previous years and was excluded (mean measured JJA albedo for 2012 was 0.99, 3.5 standard deviations above the mean 2000–2011 value of 0.64). Measured albedo at Crawford Point-2 undergoes a step change after 2004 (mean albedo is 0.81 ± 0.03 for 2000–2004 and 0.90 ± 0.04 for 2005–2010) and therefore we excluded data after 2004, as was done by Stroeve et al. (2013). At the stations NASA-U and NGRIP, leveling errors produce a low bias in upward radiation for all years (Stroeve et al., 2013) resulting in measured albedo values that are unrealistically low for snow outside of the ablation zone (0.30 ± 0.01 at NASA-U and 0.33 ± 0.01 at NGRIP), and are therefore excluded. At the Peterman Glacier and Peterman ELA,

TCD
8, 3733–3783, 2014

missing MODIS data prevented us from including all weather station data in this analysis.

As in the case of the original MAR albedo data, in situ measurements also include measurements made during cloudy conditions while MODIS albedo data do not. Given a lack of available measurements, we do not explicitly correct in situ data for the presence of clouds in this study, but only consider data where coincident satellite and in situ measurements are available. Stroeve et al. (2013) applied a correction to GC-Net data using a radiative transfer model, but found that the correction did not significantly impact their results.

The GC-Net LI-COR sensors are sensitive within the 0.4–1.1 µm band, and K-Transect data are collected in the 0.3–1.1 µm band. These bands are narrower than the MOD10A1 interval of 0.3–3 µm and the MCD43 shortwave albedo interval of 0.3–5 µm, and the interval of 0.3–2.8 µm over which albedo is calculated in the MAR model. GC-Net incoming and outgoing radiation values are calibrated to represent radiation for a spectral interval of 0.28 to 2.8 µm (Wang and Zender, 2009). However, because snow has a high spectral reflectance over the 0.3 to 1.1 µm interval, and a much lower reflectance above 1.1 µm, measured albedo over the smaller interval will be higher for snow-covered areas (Stroeve et al., 2005). Stroeve et al. (2005) compared albedo derived with GC-Net LI-COR pyranometers to measurements from pyranometers with a larger spectral range, and found that the smaller wavelength interval results in a positive albedo bias of between 0.04 and 0.09, for GC-Net data relative to MODIS albedo, depending on the location and time period (Stroeve et al., 2005). This bias likely also applies to K-Transect measurements, as the spectral sensitivity at K-Transect sites is comparable to the sensitivity at GC-Net locations. Because this bias may be smaller or larger depending on multiple factors, we do not apply any correction here, but provide an indication of spatial variability of this bias in Sect. 4.2.1 by comparing MCD43A3 visible albedo (0.3–0.7 mm) with MCD43A3 shortwave (0.3–5.0 mm) albedo.

TCD
8, 3733–3783, 2014

3 Results

3.1 Albedo spatial variability

We first examine spatial variations in mean 2000–2013 JJA MODIS daily (MOD10A1) and 16 day (MCD43A3) shortwave BSA albedo, as well as clear-sky albedo from MAR v3.2. We focus on the JJA period because MODIS data are less reliable during other months, when solar zenith angles are high, as discussed by Box et al. (2012), and because this is the period when surface albedo is likely to have the largest impact on SMB. Figure 2 shows mean 2000–2013 GrIS JJA albedo for MOD10A1, MCD43A3 and MAR v3.2. Table 2 provides mean albedo for each product within the ablation and accumulation zones. All three datasets show coherent spatial patterns that are consistent with previous studies (e.g., Box et al., 2012), with low-elevation areas in the ablation zone dominated by lower albedo values (< 0.7 on average) due to the presence of meltwater and bare ice, and high elevation areas by relatively higher albedo (> 0.75). The most obvious discrepancy between all datasets occurs north of 70° N, where the MOD10A1 daily product exhibits an increase in albedo with latitude, while MCD43A3 points to the opposite. The difference between the two satellite products (Fig. 3a) is statistically significant (at the 95 % confidence level) above 70° N, reaching ~ 0.08 (for albedo ranging between 0 and 1) at the highest latitudes.

The pattern of differences between MAR v3.2 and the two satellite products (Fig. 3b and c) exhibits a higher degree of spatial variability when compared to Fig. 3a. Because any systematic biases in the satellite products are likely to be relatively consistent across space (at least as a function of longitude), it is likely that MAR v3.2 biases contribute to some of the differences seen in Fig. 3b and c. Within the accumulation zone south of 70° N, MAR v3.2 albedo (0.77 on average) is comparable to MODIS albedo (average of 0.78 for MOD10A1 and 0.77 for MCD43A3). At low elevation areas, especially along the west coast ablation zone, MAR v3.2 overestimates albedo (up to ~ 0.1) relative to both satellite products. The mean ablation zone albedo from MOD10A1 (0.68 ± 0.07) is identical to MAR mean ablation zone albedo (Table 2), de-

TCD
8, 3733–3783, 2014

spite the large positive bias in MAR albedo within the west coast ablation zone that can be seen in Fig. 3. This is likely a result of a positive bias for MOD10A1 at high latitudes, as will be discussed further below. For areas north of 70° N, the discrepancy between satellite products makes it impossible to determine the magnitude and direction of MAR biases.

Spatial variations in albedo are further examined in Fig. 4, in which mean 2000–2013 JJA albedo for MAR and the MODIS products is plotted as a function of elevation (binned into 150 m segments) and latitude (binned into 2° segments). MAR, MOD10A1 and MCD43A3 show a similar logarithmic dependence of albedo with elevation; below 2000 m, albedo increases relatively rapidly with elevation (both MAR and the MODIS products show a statistically significant albedo increase of ~ 0.01 to ~ 0.02 per 100 m increase in elevation), while above 2000 m, the change is smaller (no statistically significant increase for MAR, and an increase of ~ 0.002 to ~ 0.003 per 100 m for both MODIS products). The discrepancies between datasets north of 70° N are evident in Fig. 4b: MCD43A3 decreases with latitude while MOD10A1 increases, and MAR v3.2 shows little change.

Data from in situ stations are compared with MODIS and MAR albedo values that are coincident in space and time in Table 3. Data have been spatially aggregated into ablation and accumulation zones of the GrIS defined by MAR v3.2, and temporally averaged over the same 16 day periods as the MCD43A3 product. In this case, we compare in situ measurements with MODIS data for the pixel closest to each weather station using the original (463 m × 463 m) MODIS grid, and do not average data to the MAR grid (25 km × 25 km). For locations in the ablation zone, in situ mean albedo (0.56 ± 0.08) is higher than MOD10A1 albedo (0.51 ± 0.09) and MCD43A3 albedo (0.50 ± 0.07), and is comparable with MAR v3.2 clear sky mean albedo for sectors classified as ice-covered (0.57 ± 0.07). Within the accumulation zone, in situ albedo is larger by 0.01 to 0.06 relative to MAR and the MODIS products. These results are consistent with a positive bias in GC-Net measurements identified by Stroeve et al. (2005). Given that GC-Net albedo values are likely positively biased, and MAR mean ablation zone albedo

TCD
8, 3733–3783, 2014

values are close to GC-Net values, MAR is also likely positively biased in the ablation zone.

In Fig. 5, we show mean 2000–2012 albedo for selected individual stations in the accumulation zone as a function of latitude, along with 2000–2012 values for all MODIS and MAR grid boxes in the accumulation zone. We only show stations for which at least 7 years of data are available for 2000–2012. Error bars on station measurements indicate the range of biases (0.04 to 0.09) that have been observed by Stroeve et al. (2005). Figure 5 and Table 3 indicate that MOD10A1 accumulation zone measurements are comparable to uncorrected GC-Net data north of 70° N (within 0.01 for aggregated station data). This suggests that the MOD10A1 may also be positively biased north of 70° N. Table 3 indicates that GC-Net albedo at stations north of 70° N is on average larger by 0.02 relative to stations south of 70° N, suggesting that GC-Net albedo does not confirm the decrease in albedo with latitude indicated by MCD43A3. It appears possible from Fig. 5 that the bias at GC-Net sites could increase with latitude, rendering GC-Net measurements comparable to MCD43A3 measurements. Through an examination of MCD43A3 visible and shortwave albedo we show that this is not likely to be the case (Sect. 4.2.1). Therefore, of the four datasets examined, only MCD43A3 appears to exhibit a decrease with latitude above 70° N.

3.2 Albedo temporal variability

The standard deviation of albedo time-series provides information on the magnitude of its temporal variability. Figure 6 shows maps of 2000–2013 JJA standard deviations for MAR and the two MODIS products, over the 16 day MCD43A3 periods (Fig. 6a–c) as well as for daily periods (Fig. 6d and e). Figure 6 and Table 2 indicate that within the low elevation ablation zone of the ice sheet, both MAR and the MODIS products exhibit a relatively high standard deviation (0.07 on average for 16 day periods). At high elevations, variability is smaller (0.02 to 0.03 on average for 16 day periods). The MCD43A3 and MOD10A1 products show similar spatial patterns of standard deviation when the daily product is averaged over 16 day MODIS periods. Table 2 suggests

TCD
8, 3733–3783, 2014

that MAR v3.2 ablation zone temporal variability is identical to MODIS variability on average, but Fig. 6 indicates that there are locations, particularly within the west coast ablation zone, where MODIS variability is considerably higher. MAR v3.2 albedo variability in low elevation areas reaches a maximum of 0.09, while MODIS variability for the same regions is 0.15 at maximum. At a daily temporal resolution, MOD10A1 daily variability in the ablation zone (0.17 maximum, 0.07 on average) is considerably larger than the variability of MAR v3.2 albedo (0.12 maximum, 0.04 on average). As will be discussed in Sect. 4.2, this may be the result of a positive bias in bare-ice albedo from MAR, but may also be associated with errors introduced by cloud artifacts in the MOD10A1 product. For the accumulation zone, the standard deviation of albedo for MAR and MODIS generally falls within the 16 day uncertainty of 0.04 for MCD43A3 high-quality albedo and daily uncertainty of 0.067 for MOD10A1 albedo estimated by Stroeve et al. (2005, 2006). This limits the comparison among MAR and the MODIS products for high elevations.

Figure 7 shows maps of correlations (on a pixel by pixel basis) between the two MODIS products, and between MAR and each of the MODIS products. For areas south of 70° N and in the ablation zone north of 70° N, the two MODIS products are highly correlated (for MCD43A3 16 day periods, $r^2 > 0.5$), but in the accumulation zone north of 70° N this correlation decreases. Maps of correlation between MAR and MODIS (Fig. 7b and c) indicate that MAR v3.2 captures more than 50 % of the ablation zone variability captured by satellite products for 16 day periods and more than 25 % for daily periods. It is, however, important to note that the daily variability from MOD10A1 is partially driven by cloud artifacts retained in the MOD10A1 product (Box et al., 2012). Within the accumulation zone, correlation between MAR and MODIS products is generally poor ($r^2 < 0.2$) and not significant at the 95 % confidence level. Again, in this region, variability is smaller than the assumed uncertainty for MCD43A3.

TCD
8, 3733–3783, 2014

3.3 Albedo spatio-temporal variability

The consistency of spatio-temporal variability in albedo between MODIS products and between MAR and MODIS prodcuts is investigated further by plotting scatter plots for all 2000–2013 JJA albedo values (Fig. 8). The scatter plots are consistent with conclusions drawn from previous analyses. For example MCD43A3 albedo is lower (by 0.03 on average) compared to MOD10A1 albedo (Fig. 8a), consistent with the significant difference between the products at high latitudes seen in Fig. 3a. There is a fairly good correlation between MCD43A3 and MOD10A1 (r^2 = 0.66) and the slope of the best linear fit (0.83) is close to 1.

When MAR is compared with MCD43A3 and MOD10A1 over 16 day periods (Fig. 8b and c), the correlation between MAR and satellite data is as good or better than the correlation between MOD10A1 and MCD43A3 (r^2 = 0.66 vs. MOD10A1 and 0.81 vs. MCD43A3). However, there is less agreement about the 1 : 1 line; a linear fit reveals a slope of 0.58 for MAR vs. MCD43A3 and 0.51 for MAR vs. MOD10A1. MAR overestimates low values of albedo (below 0.6) relative to satellite data, which is consistent with the apparent positive MAR bias in the ablation zone seen in Fig. 3b and c. On a daily basis, there is a poor agreement between MAR and MOD10A1 (Fig. 8d, r^2 = 0.35), consistent with the poor correlations observed in Fig. 7d. (Note that MOD10A1 albedo is only accurate to two decimal places, resulting in the apparent vertical lines in Fig. 8d.)

Scatter plots of 2000–2012 JJA albedo values for both satellite products and MAR v3.2 vs. all weather station measurements (Fig. 9) indicate a strong correlation between in situ data and the two satellite products over 16 day periods (Fig. 9a and b; r^2 = 0.80 for MOD10A1, r^2 = 0.81 for MCD43A3), as well as a good agreement about the 1 : 1 line (slope = 0.95 for MOD10A1 and 0.88 for MCD43A3). MAR agrees reasonably well with in situ data, but the correlation is lower (r^2 = 0.78), and the slope (0.66) is further from 1. Again, it appears that MAR also overestimates low albedo values relative to in situ measurements, in consistency with Fig. 8b and c.

TCD
8, 3733–3783, 2014

On a daily basis, MOD10A1 albedo exhibits a nearly 1 : 1 relationship with daily in situ albedo (Fig. 9d; slope = 0.99), although there is increased scatter (r^2 = 0.75) due to higher variability on daily timescales, as shown in Fig. 6. Similarly, when MAR is compared with daily in situ measurements, the correlation is lower relative to the 16 day comparison (r^2 = 0.74), while the slope of the best fit line does not change substantially (slope = 0.65).

In Figs. 8 and 9, blue points indicate locations within the MAR-defined accumulation zone. All datasets agree that spatiotemporal variability of albedo is higher in the ablation zone (where the standard deviation of albedo is ∼ 0.13) than in the accumulation zone (standard deviation of ∼ 0.04). This is to be expected, given that the ablation zone experiences a substantial seasonal cycle in melting.

3.4 Greenland Ice Sheet albedo trends

Box et al. (2012) investigated changes in GrIS albedo using the MOD10A1 albedo product, finding that between 2000 and 2012, surface albedo decreased over almost the entire ice sheet. Here, we build on the analysis of Box et al. (2012) and extend the analysis to include MCD43A3, MAR and in situ JJA data for the period 2000–2013. Maps of GrIS trends for 2000–2013 for MCD43A3, MOD10A1, and MAR are shown in Fig. 10 and timeseries' of annual average albedo are shown in Fig. 11. MAR, MCD43A3, and MOD10A1 consistently agree that there has been a significant decrease in albedo within the ablation zone over 2000–2013, and that the largest decreases in albedo have occurred below 2000 m a.s.l. MCD43A3 shows a decrease of up to −0.1 per decade for pixels in the ablation zone, as does MOD10A1 (both products show a decrease of −0.06 per decade for the entire zone). MAR agrees with these trends, but the overall magnitude is smaller (−0.03 per decade for the entire zone).

Within the accumulation zone, the MAR disagrees with the two MODIS products as to the direction and magnitude of trends. MCD43A3 shows a decrease of −0.03 per decade on average, and MOD10A1 trends are somewhat larger (−0.04 per decade on average), while for MAR, trends are generally not statistically significant at the 95 %

TCD
8, 3733–3783, 2014

level for grid boxes above 2500 m a.s.l., and are slightly positive in some high-elevation areas.

We also compare decadal trends at weather stations where there is a record of at least 9 years in Table 4. For locations within the GrIS ablation zone, trends at weather stations are consistent with significant decreases in albedo indicated by MODIS and MAR over the periods specified (2000–2012 or 2004–2012). The magnitude of the trends varies between datasets at individual stations. These differences can be attributed in part to the high spatio-temporal variability of albedo within the ablation zone. This can potentially lead to trends at a weather station that are substantially different from trends within a 500 m MODIS grid box containing the location of that weather station. At higher elevations, this factor is less important as there is less spatio-temporal variability in albedo (as shown in Figs. 8 and 9). Within the accumulation zone, trends at weather stations are generally within ±0.01 per decade of MAR trends; they are generally not statistically significant and are close to zero, unlike MODIS estimates, which show trends ranging between −0.01 and −0.07 per decade.

4 Discussion

4.1 Albedo properties of the Greenland Ice Sheet captured by all datasets

The results presented above highlight certain features of Greenland ice sheet albedo variability that are common to in situ, satellite, and model data. All datasets capture general spatial patterns of low albedo in the ablation zone, which increases with increasing elevation below ~ 2000 m and is relatively insensitive to elevation at higher elevations (Figs. 2 and 4a, Table 3). This spatial variability is consistent with the presence of meltwater and bare ice exposure at low elevations, which are a function of surface air temperatures, and therefore elevation. At high-elevation areas that are permanently snow covered, particularly at northern sites, melting is infrequent (Nghiem et al., 2012) and albedo variability is primarily associated with accumulation and subsequent dry

TCD
8, 3733–3783, 2014

snow grain size metamorphism. Low elevation melting and bare ice exposure during warm summer months reduces surface albedo relative to snow albedo, resulting in a seasonal cycle that increases local variability. As Fig. 6 and Tables 2 and 3 show, all datasets show higher variability in the ablation zone (where the mean standard deviation of albedo at in situ stations ranges between ±0.06 and ±0.09) relative to the accumulation zone (where standard deviation range between ±0.02 and ±0.04).

As noted in Sect. 3.5, all datasets agree that there has been a significant decline in ablation zone albedo between 2000 and 2013. These trends in surface albedo are associated with increased melting and bare ice exposure resulting in a declining ablation zone SMB, captured by models (Fettweis et al., 2011; Ettema et al., 2009) and in situ observations (van de Wal et al., 2012), and are driven by warmer regional atmospheric air temperatures, associated with atmospheric circulation changes (Fettweis et al., 2013a; Häkkinen et al., 2014).

4.2 Insights from differences between datasets

4.2.1 Variation of albedo with latitude

Results from Sect. 4.1 indicate that above 70° N, MOD10A1 shows an increase in albedo with latitude, MCD43A3 exhibits a decrease, MAR shows little change, and there is also a small increase with latitude at local weather stations (Figs. 2, 4b, 5, Table 3).

In Sect. 3.1 we mentioned the possibility that the bias at GC-Net stations could vary with latitude, rendering corrected GC-Net mean 2000–2013 JJA albedo comparable to MCD43A3 albedo. In order to indicate how the GC-Net albedo bias is likely to vary spatially, Fig. 12 shows the difference between MCD43A3 visible BSA (for the interval 0.3–0.7 µm) and MCD43A3 shortwave BSA (for the interval 0.3–5.0 µm). The difference between MCD43A3 visible and MCD43A3 shortwave BSA (which ranges between 0.1 and 0.2) is larger than the biases observed by Stroeve et al. (2005) at GC-stations (which range between 0.04 to 0.09), likely because the MCD43A3 visible wavelength

TCD
8, 3733–3783, 2014

interval is smaller than that for GC-Net stations. The difference is lowest in the ablation zone where bare ice is exposed during summer months, is largest in regions where melting occurs, but bare ice exposure is infrequent, and is relatively small at high elevations.

Because ice does not exhibit the spectral dependence of albedo that snow does (Hall and Martinec, 1985), the difference between MCD43A3 visible and shortwave albedo is lower in the ablation zone, particularly along the west coast of Greenland, where bare ice is exposed during summer. In locations where melting occurs, snow grains tend to be larger because of constructive metamorphism, reducing reflectance mostly in the near infrared band (Wiscombe and Warren, 1980), hence resulting in a larger difference between visible and near infrared reflectance. At high elevations, there is little or no melting, and therefore a smaller difference between albedo in different bands. The difference is not a function of latitude, but rather appears to be related to surface properties. This suggests that in situ albedo values do not exhibit the decrease of albedo with latitude suggested by MCD43A3.

Theoretically, snow albedo is expected to increase with increasing solar zenith angle, particularly for high solar zenith angles (Wiscombe and Warren, 1980) and therefore will increase slightly with latitude at high latitudes, as long as other factors do not contribute to lower albedo values. Wang and Zender (2009) compared 16 day MCD43C3 albedo with GC-Net measurements and suggest that the MCD43C3 product is unrealistic at higher latitudes, in particular for solar zenith angles > 55°. (The MCD43C3 product differs from the MCD43A3 product used here only in its grid.) Schaaf et al. (2011) and Stroeve et al. (2013) suggest that the findings of Wang and Zender (2009) are inaccurate, partially because they did not separate results for high- vs. low-quality albedo. We have considered this in our study: results for all MCD43A3 data are shown along with good quality MCD43A3 data in Fig. 4b. While the use of only good quality data increases MCD43A3 albedo above 70° N, it does not fundamentally change the dependency of MCD43A3 albedo on latitude. For MOD10A1, excluding low quality data has little effect on the binned values.

TCD
8, 3733–3783, 2014

It should also be noted that the MOD10A1 product, to the contrary, may be positively biased above 70° N, given that it is comparable with uncorrected in situ data, which are likely positively biased (Fig. 5). We do not have a reasonable explanation for this potential bias, but as noted by Box et al. (2012), the MOD10A1 product contains artifacts that have not been removed during quality control, even for "good quality" data. Box et al. (2012) also suggest that values of albedo from MOD10A1 above 0.84 are unrealistic for snow under clear-sky conditions.

4.2.2 Differences between MAR v3.2 and observations

The major difference between MAR v3.2 albedo and observed albedo is an overall positive bias in the ablation zone. This bias can be seen most clearly as a difference of ∼ 0.1 between MAR and the two MODIS products along the west coast ablation zone in Fig. 3b and c, and in a difference between MAR and both MODIS products of 0.06 at in situ stations (with low elevation stations mostly located in the west coast ablation zone). Mean ablation zone albedo from local stations is also comparable with coincident MAR albedo (Table 3), but local station measurements are likely positively biased, further confirming a positive MAR bias in this area.

Scatter plots of ablation zone albedo appear to confirm this: when MAR is compared with both MODIS data and in situ measurements (Figs. 8b, c and 9c) the result is a best fit line with a slope smaller than one. Additionally in the same area where MAR appears positively biased in the west coast ablation zone, MODIS exhibits relatively high variability compared with MAR (as discussed in Sect. 3.3; Fig. 6).

The positive bias from MAR v3.2, as well as the relatively low modeled variability in the ablation zone is the result of the albedo values set for bare ice (ranging between 0.45 and 0.55) in MAR v3.2 that may be too high, as will be discussed further in the following section. A bare ice albedo that is too high will, indeed, lead to a smaller difference between the albedo values of melting snow and bare ice, reducing temporal variations in ablation zone albedo. Also, MAR v3.2 albedo is only a function of accumulated meltwater and does not explicitly take into account the presence of dust, surface

TCD
8, 3733–3783, 2014

lakes and surface streams, including the West Greenland "dark zone" (van de Wal and Oerlemans, 1994; Wientjes and Oerlemans, 2010), which reduces bare ice albedo and likely introduces increased ablation zone albedo variability.

4.2.3 MAR v3.2 vs. MAR v2.0 albedo

In order to further examine some of the discrepancies between MAR and observations, we find it useful to examine differences between MAR v3.2 and a previous version (MAR v2.0), which has been validated against satellite and in situ data (e.g. Fettweis et al., 2005, 2011) and used for making future projections (Fettweis et al., 2013b; Tedesco and Fettweis, 2012). Comparisons are conducted for the 2000–2012 period, as MAR v2.0 data are available only through 2012. A major difference between MAR v3.2 and MAR v2.0 is in the scheme for calculating the albedo of bare ice. As noted in Sect. 2.2, MAR v2.0 assumes a fixed value of 0.45 in the case where surface densities exceed 920 kg m^{-3}, while in MAR v3.2, bare ice albedo ranges between 0.45 and 0.6 as a function of surface melt.

In Fig. 13, we show scatter plots for MAR vs. MODIS 2000–2012 JJA ablation zone albedo on 16 day timescales for both versions of MAR along with frequency histograms of albedo values for MAR and the two MODIS products, and distributions of the best-fit of these histograms obtained using maximum likelihood estimation. Statistics for the mean (μ) and standard deviation (σ) of these best-fit distributions are shown in Table 5. MAR v2.0 exhibits a clustering of albedo values above 0.65 and below 0.6, resulting in a bimodal distribution of albedo values (Fig. 13a). MCD43A3 also shows a bimodal distribution of albedo, but the distributions of the two modes overlap, and there is a wider range of low albedo values (σ = 0.10 for MCD43A3 and 0.05 for MAR for the best fit of the lower albedo peak). The MAR v3.2 distribution exhibits a slightly wider range of low albedo values (σ = 0.06 for the low albedo peak) with a mean that is positively shifted relative to MAR v2.0 (μ = 0.61 vs. 0.50) (Fig. 13b). MOD10A1 does not appear to exhibit a bimodal distribution with two distinct peaks, but the best-fit curve agrees qualitatively with the observed distribution (Fig. 13c). The higher uncertainty

TCD
8, 3733–3783, 2014

and therefore increased variability for the MOD10A1 product (Fig. 6; Stroeve et al., 2006) may possibly mask the two peaks of the distribution. Indeed, the best-fit bimodal distribution from MOD10A1 has a higher standard deviation of albedo for the higher albedo peak (σ = 0.06 for MOD10A1 vs. 0.04 for MCD43A3).

The bimodal distribution of albedo appears to be related to the presence of two main surface types within the ablation zone, ice (and firn) and snow. Pixels classified by MAR as having bare ice (or firn, surface density > 830 kg m^{-3}) for at least 8 days of each 16 day period are shown in red in Fig. 13, and the location of these points coincides with one of two peaks in the bimodal distributions. MAR v2.0 logically exhibits a smaller range of low albedo values compared with MODIS, given that its bare-ice albedo is fixed at 0.45. An examination of Fig. 13 indicates that the low albedo peak for MAR v3.2, for which bare-ice albedo ranges between 0.45 and 0.6, is closer to being normally distributed compared with the peak for MAR v2.0, and therefore better matches the distribution from MCD43A3. However, the MAR v3.2 parameterization overestimates the bare ice albedo, as already discussed, and still does not fully capture the variability in the low albedo peak for MODIS albedo (σ = 0.06 for MAR v3.2 and σ = 0.10 for both MODIS products).

We compare MAR v2.0 mean 2000–2012 clear-sky JJA albedo with albedo from MAR v3.2 and MODIS in Fig. 14a–c. Figure 14a shows that MAR v3.2 albedo is significantly larger in the ablation zone compared with MAR v2.0. Rather than being positively biased relative to MODIS (as is the case for MAR v3.2 as shown in Fig. 3), MAR v2.0 albedo is either negatively biased or is not significantly different from MODIS data. The difference in albedo scheme is the major difference between MAR v3.2 and MAR v2.0, and it results in a significant difference in SMB, as shown in Fig. 14d. The average ablation zone JJA SMB for MAR v3.2 is higher by 0.53 mWE yr^{-1} compared with the average for MAR v2.0, a considerable fraction (roughly 25 %) of the mean ablation zone JJA SMB from MAR v3.2, which is on average −2.02 mWE yr^{-1} for the period 2000–2013. This highlights the importance of a model's albedo scheme in determining the ablation rate and size of the ablation zone (van Angelen et al., 2012). The results

TCD
8, 3733–3783, 2014

suggest that although MAR v3.2 appears to correct a low albedo bias present in MAR v2.0, and introduces a more realistic distribution of bare ice albedo, it also introduces a positive albedo bias, particularly along the west coast ablation zone, which is rich in impurities. A reduction of the minimum bare ice albedo (0.45 currently) in the next MAR version may reduce this bias by more realistically representing the GrIS surface.

4.2.4 Discrepancies in ablation zone trends

As noted in Sect. 3.5, there is a discrepancy between different datasets regarding albedo trends in the accumulation zone of the ice sheet. MOD10A1 and MCD43A3 show significant decreases in accumulation zone albedo (−0.04 to −0.03 per decade) while MAR v3.2 trends are generally not statistically significant, and in situ trends are generally small (not larger than −0.01 per decade) or not significant.

A possible explanation for this discrepancy is that MODIS trends are negatively biased as a result of declining instrument sensitivity of the MODIS sensors (Wang et al., 2012). In particular, a larger degradation has been observed for the MODIS Terra satellite (Wang et al., 2012). The MCD43A3 product uses data from both the Terra and Aqua satellites, while MOD10A1 only uses data from Terra. This could potentially explain the larger trends for MOD10A1 relative to MCD43A3 (Table 4, Fig. 10). Box et al. (2012) conclude that declining instrument sensitivity does not substantially affect GrIS albedo trends, because they find larger trends in GC-Net data relative to MOD10A1 for 70 % of cases where trends are deemed to be significant. We do not find JJA GC-Net trends larger than those of MODIS, except in ablation zone areas with high local variability, in contrary to the findings of Box et al. (2012). The analysis performed here is somewhat different from that employed by Box et al. (2012). Differences in trends may result from the fact that here we have focused on trends for the entire JJA period rather than on monthly trends, and calculate trends for 16 day albedo values rather than calculating a monthly albedo from integrated fluxes over a 1 month period, as was done by Box et al. (2012).

TCD
8, 3733–3783, 2014

We also investigated the possibility that the smaller spectral interval of GC-Net data influences trends (not shown here). We find that MCD43A3 visible albedo shows differences of smaller than ±0.05 per decade compared with MCD43A3 shortwave and the differences are not statistically significant. The largest differences are found in the west coast ablation zone. This is likely associated with more frequent bare ice exposure, which substantially reduces visible albedo, but does not have as large of an effect on near infrared albedo, due to the low reflectance of snow at near infrared wavelengths. This may therefore have some impact on ablation zone stations that experience bare ice exposure (e.g. JAR2 and S9) contributing to larger trends observed at these locations relative to MAR and MODIS (Table 4), but again, the overall impact is small.

We are not able to prove that the larger trends from MODIS are associated with declining instrument sensitivity, as this analysis is outside the scope of this study. However, the findings of this study seem consistent with this possibility and this is suggested as a topic for future research.

5 Conclusions

We have examined spatio-temporal variability and trends in GrIS albedo using in situ measurements, satellite products obtained from MODIS data, and outputs of a regional climate model (MAR v3.2). The results presented here reveal areas of agreement as well as discrepancies between observational and model estimates of GrIS albedo spatio-temporal variability. Examining all of these datasets concurrently reveals information about the GrIS albedo and potential biases that would not be revealed by examining any of the datasets individually.

The results presented here show that albedo varies spatially as a function primarily of surface properties, in particular melting and bare-ice exposure in the ablation zone. These factors are also associated with temporal variations in albedo, resulting in high variability in low elevation regions. The differences in variations with latitude indicated by satellite products appear likely to be a function of inaccuracies associated with the

TCD
8, 3733–3783, 2014

products themselves, rather than a record of actual variations in surface albedo, particularly as the two products are derived from the same MODIS sensors.

Both satellite products and MAR model data (for v2.0 and v3.2) suggest that there is a bimodal distribution of surface albedo within the ablation zone of the ice sheet. Based on model results, we infer that this distribution is associated with the presence of two primary surface types within the ablation zone, snow and bare ice. The model's inability to capture the full range of low elevation albedo leads to inaccuracies in the representation of spatiotemporal variations in albedo, which can substantially impact the representation of SMB. The MAR version examined here (v3.2) appears to better represent the full range of bare-ice albedo in the ablation zone relative to a previous version (v2.0), but a lower minimum bare ice albedo value (as is implemented in the next version of MAR, v3.4) may produce results that are more consistent with observations.

A comparison between multiple datasets indicates a statistically significant decrease in ablation zone albedo over the period 2000–2013 that is consistent with previous studies (Box et al., 2012; Tedesco et al., 2011, 2013). This decrease is consistent with a coincident decline in ablation zone SMB recorded by both models and observations (e.g. Fettweis et al., 2011; Ettema et al., 2009; van de Wal et al., 2012). Our results are inconclusive regarding high elevation trends in albedo; we observe inconsistencies between satellite-derived trends and trends obtained from in situ measurements and MAR v3.2 results. We are therefore unable to confirm previously reported decreases in surface albedo at high elevations.

Future research should be directed towards understanding the reasons for discrepancies between datasets, in order to better understand changes in GrIS albedo. This includes resolving discrepancies between datasets regarding high-elevation trends, and discrepancies in mean satellite-derived surface albedo at high latitudes. Models such as MAR appear to be effective at capturing surface albedo, but refinements are necessary for representation of surface albedo in low elevation areas. (In particular, the representation of bare ice albedo is critical.) Sensitivity studies, such as those performed

TCD
8, 3733–3783, 2014

by van Angelen et al. (2012) of the impact of surface albedo on SMB variability, may help to quantify the accuracy with which surface albedo must be modeled for a given region. Analysis of spatiotemporal variations in albedo across different spatial scales may also become increasingly important as models operate at higher spatial resolutions. Given the strong relationship between surface albedo and SMB, these future studies are crucial for efforts aiming at estimating and predicting the impact of current and future climate change on GrIS SMB.

Acknowledgements. This research is supported by NSF Grant 0909388. In situ data along the K-transect are financed over time by Utrecht University, and several grants from the Polar Program of the Netherlands Organization for Scientific Research (NWO) including the Spinoza Program and the Royal Academy of Sciences (KNAW). The authors would like to thank Rajashree Datta for comments and suggestions. Part of this work was performed while Marco Tedesco was serving as Program Director at the National Science Foundation.

References

Bamber, J. L., Ekholm, S., and Krabill, W. B.: A new, high-resolution digital elevation model of Greenland fully validated with airborne laser altimeter data, J. Geophys. Res., 106, B4, 6733–6745, 2001.

Bamber, J. L., Griggs, J. A., Hurkmans, R. T. W. L., Dowdeswell, J. A., Gogineni, S. P., Howat, I., Mouginot, J., Paden, J., Palmer, S., Rignot, E., and Steinhage, D.: A new bed elevation dataset for Greenland, The Cryosphere, 7, 499–510, doi:10.5194/tc-7-499-2013, 2013.

Box, J. E. and Rinke, A.: Evaluation of Greenland Ice Sheet surface climate in the HIRHAM Regional Climate Model using automatic weather station data, J. Climate, 16, 1302–1319, 2002.

Box, J. E., Bromwich, D. H., Veenhuis, B. A., Bai, L.-S., Stroeve, J. C., Rogers, J. C., Steffen, K., Haran, T., and Wang, S.-H.: Greenland Ice Sheet surface mass balance variability (1988–2004) from calibrated Polar MM5 output, J. Climate, 19, 2783–2800, 2006.

Box, J. E., Fettweis, X., Stroeve, J. C., Tedesco, M., Hall, D. K., and Steffen, K.: Greenland ice sheet albedo feedback: thermodynamics and atmospheric drivers, The Cryosphere, 6, 821–839, doi:10.5194/tc-6-821-2012, 2012.

TCD
8, 3733–3783, 2014

Brun, E., David, P., Sudul, M., and Brunot, G.: A numerical model to simulate snow-cover stratigraphy for operational avalanche forecasting, J. Glaciol., 38, 128, 13–22, 1992.
Ettema, J., van den Broeke, M. R., van Meijgaard, E., van de Berg, W. J., Bamber, J. L., Box, J. E., Bales, R. C.: Higher surface mass balance of the Greenland ice sheet revealed by high-resolution climate modeling, Geophys. Res. Lett., 36, L12501, doi:10.1029/2009GL038110, 2009.
Fettweis, X.: Reconstruction of the 1979–2006 Greenland ice sheet surface mass balance using the regional climate model MAR, The Cryosphere, 1, 21–40, doi:10.5194/tc-1-21-2007, 2007.
Fettweis, X., Gallée, H., Lefebre, F., and van Ypersele, J.-P.: Greenland surface mass balance simulated by a regional climate model and comparison with satellite-derived data in 1990–1991, Clim. Dynam., 24, 623–640, 2005.
Fettweis, X., van Ypersele, J.-P., Gallée, H., Lefebre, F., and Lefebvre, W.: The 1979–2005 Greenland ice sheet melt extent from passive microwave data using an improved version of the melt retrieval XPGR algorithm, Geophys. Res. Lett., 34, L05502, doi:10.1029/2006GL028787, 2007.
Fettweis, X., Tedesco, M., van den Broeke, M., and Ettema, J.: Melting trends over the Greenland ice sheet (1958–2009) from spaceborne microwave data and regional climate models, The Cryosphere, 5, 359–375, doi:10.5194/tc-5-359-2011, 2011.
Fettweis, X., Hanna, E., Lang, C., Belleflamme, A., Erpicum, M., and Gallée, H.: *Brief communication* "Important role of the mid-tropospheric atmospheric circulation in the recent surface melt increase over the Greenland ice sheet", The Cryosphere, 7, 241–248, doi:10.5194/tc-7-241-2013, 2013a.
Fettweis, X., Franco, B., Tedesco, M., van Angelen, J. H., Lenaerts, J. T. M., van den Broeke, M. R., and Gallée, H.: Estimating the Greenland ice sheet surface mass balance contribution to future sea level rise using the regional atmospheric climate model MAR, The Cryosphere, 7, 469–489, doi:10.5194/tc-7-469-2013, 2013b.
Franco, B., Fettweis, X., Lang, C., and Erpicum, M.: Impact of spatial resolution on the modelling of the Greenland ice sheet surface mass balance between 1990–2010, using the regional climate model MAR, The Cryosphere, 6, 695–711, doi:10.5194/tc-6-695-2012, 2012.
Gallée, H.: Air–sea interactions over Terra Nova Bay during winter: simulation with a coupled atmosphere-polynya model, J. Geophys. Res., 102, D12, 13835–13849, 1997.

TCD
8, 3733–3783, 2014

Gallée, H. and Schayes, G.: Development of a three-dimensional meso-γ primitive equation model: katabatic winds simulation in the area of Terra Nova Bay, Antarctica, Mon. Weather Rev., 122, 671–685, 1994.

Greuell, W. and Konzelman, T.: Numerical modelling of the energy balance and the englacial temperature of the Greenland Ice Sheet. Calculations for the ETH-Camp location (West Greenland, 1155 m.a.s.l.), Global Planet. Change, 9, 91–114, 1994.

Häkkinen, S., Hall, D. K., Shuman, C. A., Worthen, D. L., and DiGirolamo, N. E.: Greenland ice sheet melt from MODIS and associated atmospheric variability, Geophys. Res. Lett., 41, 1600–1607, 2014.

Hall, D. K. and Martinec, J.: Remote Sensing of Ice and Snow, Chapman and Hall, London, 1985.

Hall, D. K., Salomonson, V. V., and Riggs, G. A.: MODIS/Terra Snow Cover Daily L3 Global 500 m Grid. Version 5. (Tiles h15v02, h16v02, h17v02, h16v01, h17v02, h16v00, h17v00), National Snow and Ice Data Center, Boulder, Colorado USA, 2012.

Klein, A. G. and Stroeve, J.: Development and validation of a snow albedo algorithm for the MODIS instrument, Ann. Glaciol., 34, 45–52, 2002.

Lefebre, F., Gallée, H., van Ypersele, J.-P., and Greuell, W.: Modeling of snow and ice melt at ETH Camp (West Greenland): a study of surface albedo, J. Geophys. Res., 108, 4231, doi:10.1029/2001JD001160, 2003.

Lefebre, F., Fettweis, X., Gallée, H., van Ypersele, J.-P., Marbaix, P., Greuell, W., and Calanca, P.: Evaluation of a high-resolution regional climate model simulation over Greenland, Clim. Dynam., 25, 99–116, doi:10.1007/s00382-005-0005-8, 2005.

Nghiem, S. V., Hall, D. K., Mote, T. L., Tedesco, M., Albert, M. R., Keegan, K., Shuman, C. A., DiGirolamo, N. E., and Neumann, G.: The extreme melt across the Greenland ice sheet in 2012, Geophys. Res. Lett., 39, L20502, doi:10.1029/2012GL053611, 2012.

Rae, J. G. L., Aðalgeirsdóttir, G., Edwards, T. L., Fettweis, X., Gregory, J. M., Hewitt, H. T., Lowe, J. A., Lucas-Picher, P., Mottram, R. H., Payne, A. J., Ridley, J. K., Shannon, S. R., van de Berg, W. J., van de Wal, R. S. W., and van den Broeke, M. R.: Greenland ice sheet surface mass balance: evaluating simulations and making projections with regional climate models, The Cryosphere, 6, 1275–1294, doi:10.5194/tc-6-1275-2012, 2012.

Rignot, E., Velicogna, I., van den Broeke, M. R., Monaghan, A., and Lenaerts, J.: Acceleration of the contribution of the Greenland and Antarctic ice sheets to sea level rise, Geophys. Res. Lett., 38, L05503, doi:10.1029/2011GL046583, 2011.

TCD
8, 3733–3783, 2014

Schaaf, C. B., Gao, F., Strahler, A. H., Lucht, W., Li, X., Tsang, T., Strugnell, N. C., Zhang, X., Jin, Y., Muller, J.-P., Lewis, P., Barnsley, M., Hobson, P., Disney, M., Roberts, G., Dunderdale, M., Doll, C., d'Entremont, R. P., Hu, B., Liang, S., Privette, J. L., and Roy, D.: First operational BRDF, albedo nadir reflectance products from MODIS, Remote Sens. Environ., 83, 135–148, 2002.

Schaaf, C. B., Wang, Z., and Strahler, A. H.: Commentary on Wang and Zender – MODIS snow albedo bias at high solar zenith angles relative to theory and to in situ observations in Greenland, Remote Sens. Environ., 115, 1296–1300, 2011.

Steffen, K., Box, J. E., and Abdalati, W.: Greenland Climate Network: GC-Net, in: CRREL 96-27 Special report on glaciers, ice sheets and volcanoes, trib. to M. Meier, edited by: Colbeck, S. C., US Army Cold Regions Research and Engineering Laboratory (CRREL), Hanover, New Hampshire, 98–103, 1996.

Stroeve, J., Box, J. E., Gao, F., Liang, S., Nolin, A., and Schaaf, C.: Accuracy assessment of the MODIS 16-day albedo product for snow: comparisons with Greenland in situ measurements, Remote Sens. Environ., 94, 46–60, 2005.

Stroeve, J. C., Box, J. E., and Haran, T.: Evaluation of the MODIS (MOD10A1) daily snow albedo product over the Greenland ice sheet, Remote Sens. Environ., 105, 155–171, 2006.

Stroeve, J. C., Box, J. E., Wang, Z., Schaaf, C., and Barret, A.: Re-evaluation of MODIS MCD43 Greenland albedo accuracy and trends, Remote Sens. Environ., 138, 199–214, 2013.

Tedesco, M. and Fettweis, X.: 21st century projections of surface mass balance changes for major drainage systems of the Greenland ice sheet, Environ. Res. Lett., 7, 045050, doi:10.1088/1748-9326/7/4/045405, 2012.

Tedesco, M., Serreze, M., and Fettweis, X.: Diagnosing the extreme surface melt event over southwestern Greenland in 2007, The Cryosphere, 2, 159–166, doi:10.5194/tc-2-159-2008, 2008.

Tedesco, M., Fettweis, X., van den Broeke, M. R., van de Wal, R. S. W., Smeets, C. J. P. P., van de Berg, W. J., Serreze, M. C., and Box, J. E.: The role of albedo and accumulation in the 2010 melting record in Greenland, Environ. Res. Lett., 6, 014005, doi:10.1088/1748-9326/6/1/014005, 2011.

Tedesco, M., Alexander, P., Box, J. E., Cappelen, J., Mote, T., Steffen, K., van de Wal, R. S. W., Wahr, J., and Wouters, B.: Greenland Ice Sheet, in: State of the Climate in 2012, edited by: Blunden, J. and Arndt, D., B. Am. Meteorol. Soc., 94, S121–S123, 2013.

TCD
8, 3733–3783, 2014

van Angelen, J. H., Lenaerts, J. T. M., Lhermitte, S., Fettweis, X., Kuipers Munneke, P., van den Broeke, M. R., van Meijgaard, E., and Smeets, C. J. P. P.: Sensitivity of Greenland Ice Sheet surface mass balance to surface albedo parameterization: a study with a regional climate model, The Cryosphere, 6, 1175–1186, doi:10.5194/tc-6-1175-2012, 2012.

van den Broeke, M., Bamber, J., Ettema, J., Rignot, E., Schrama, E., Jan van de Berg, W., van Meijgaard, E., Velicogna, I., and Wouters, B.: Partitioning recent Greenland mass loss, Science, 326, 984–986, doi:10.1126/science.1178176, 2009.

van den Broeke, M. R., Smeets, C. J. P. P., and van de Wal, R. S. W.: The seasonal cycle and interannual variability of surface energy balance and melt in the ablation zone of the west Greenland ice sheet, The Cryosphere, 5, 377–390, doi:10.5194/tc-5-377-2011, 2011.

van de Wal, R. S. W. and Oerlemans, J.: An energy balance model for the Greenland Ice Sheet, Global Planet. Change, 9, 115–131, 1994.

van de Wal, R. S. W., Greuell, W., van den Broeke, M. R., Reijmer, C. H., and Oerlemans, J.: Surface mass-balance observations and automatic weather station data along a transect near Kangerlussuaq, West Greenland, Ann. Glaciol., 42, 311–316, 2005.

van de Wal, R. S. W., Boot, W., Smeets, C. J. P. P., Snellen, H., van den Broeke, M. R., and Oerlemans, J.: Twenty-one years of mass balance observations along the K-transect, West Greenland, Earth Syst. Sci. Data, 4, 31–35, doi:10.5194/essd-4-31-2012, 2012.

Vernon, C. L., Bamber, J. L., Box, J. E., van den Broeke, M. R., Fettweis, X., Hanna, E., and Huybrechts, P.: Surface mass balance model intercomparison for the Greenland ice sheet, The Cryosphere, 7, 599–614, doi:10.5194/tc-7-599-2013, 2013.

Wang, D., Morton, D., Masek, J., Wu, A., Nagol, J., Xiong, X., Levy, R., Vermote, E., and Wolfe, R.: Impact of sensor degradation on the MODIS NDVI time series, Remote Sens. Environ., 119, 55–61, 2012.

Wang, X. and Zender, C. S.: MODIS snow albedo bias at high solar zenith angles relative to theory and to in situ observations in Greenland, Remote Sens. Environ., 114, 563–575, 2009.

Wientjes, I. G. M. and Oerlemans, J.: An explanation for the dark region in the western melt zone of the Greenland ice sheet, The Cryosphere, 4, 261–268, doi:10.5194/tc-4-261-2010, 2010.

Wiscombe, W. J. and Warren, S. G.: A model for the spectral albedo of snow: pure snow, J. Atmos. Sci., 37, 2712–2733, 1980.

TCD
8, 3733–3783, 2014

Zuo, Z. and Oerlemans, J.: Modelling albedo and specific balance of the Greenland ice sheet: calculations for the Søndre Strømfjord transect, J. Glaciol., 42, 305–317, 1996.

TCD
8, 3733–3783, 2014

Table 1. GC-Net and K-Transect weather stations used in this study and years of coverage.

Station Name	Coverage Period	Excluded data
Ablation Zone		
Swiss Camp (GC-Net)	2000–2003, 2005–2011	2012
JAR 1 (GC-Net)	2000–2012	
JAR 2 (GC-Net)	2000–2005, 2007, 2009–2012	
JAR 3 (GC-Net)	2000–2003	
S5 (K-Transect)	2004–2012	
S6 (K-Transect)	2004–2012	
S9 (K-Transect)	2004–2012	
Peterman ELA (GC-Net)	2012	2003, 2005
Peterman Glacier (GC-Net)	Not Used	2002–2005
Accumulation Zone, North of 70° N		
GIST (GC-Net)	2001, 2002, 2006, 2012	
Humboldt (GC-Net)	2002–2005, 2007, 2010–2012	
Summit (GC-Net)	2000–2012	
Tunu N (GC-Net)	2000–2002, 2005–2012	
NASA-E (GC-Net)	2000–2007, 2010–2012	
NEEM (GC-Net)	2006–2012	
NASA-U (GC-Net)	Not Used	2003–2012
NGRIP (GC-Net)	Not Used	2002–2004, 2007–2009
Accumulation Zone, South of 70° N		
KULU (GC-Net)	2000	
S10 (K-Transect)	2010–2012	
Crawford Point 1 (GC-Net)	2000–2004	2005–2010
Crawford Point 2 (GC-Net)	2000	
Dye-2 (GC-Net)	2000–2012	
Saddle (GC-Net)	2000–2001, 2003–2008, 2010–2012	
South Dome (GC-Net)	2003–2012	
NASA SE (GC-Net)	2000–2007, 2009–2012	
KAR (GC-Net)	2000, 2001	
Aurora (GC-Net)	Not Used	

TCD
8, 3733–3783, 2014

Table 2. Summary of mean 2000–2012 JJA Greenland ice sheet albedo, for MOD10A1, MCD43A3 BSA shortwave, and MAR clear-sky albedo, averaged within the mass balance zones shown in Fig. 1 and Table 1. Only good quality MODIS data are used here. All data have been averaged over the same 16 day periods of the MCD43A3 product. Only periods when coincident data for all datasets are available have been included.

Locations	MOD10A1	MCD43A3 BSA Shortwave	MAR Clear Sky
Ice-Sheet wide	0.77 ± 0.04	0.73 ± 0.04	0.75 ± 0.03
Ablation Zone	0.68 ± 0.07	0.63 ± 0.07	0.68 ± 0.07
Accumulation Zone	0.80 ± 0.03	0.75 ± 0.03	0.77 ± 0.02
Acc. Zone (N. of 70° N)	0.80 ± 0.03	0.75 ± 0.03	0.77 ± 0.02
Acc. Zone (S. of 70° N)	0.78 ± 0.03	0.77 ± 0.03	0.77 ± 0.02

TCD
8, 3733–3783, 2014

Table 3. Summary of mean 2000–2012 JJA albedo (and average standard deviations) at in situ stations, for MOD10A1, MCD43A3 BSA shortwave, and MAR clear-sky albedo, aggregated into the mass balance zones shown in Fig. 1 and Table 1. Only good quality MODIS data are used here. All data have been averaged over the same 16 day periods of the MCD43A3 product. Only periods when coincident data for all datasets is available have been included. The closest pixel to the in situ station is used for MAR and MODIS data.

Locations	MOD10A1	MCD43A3 BSA Shortwave	MAR Cloud-Corrected	In Situ
All stations	0.69 ± 0.06	0.67 ± 0.04	0.70 ± 0.04	0.74 ± 0.05
Ablation Zone	0.51 ± 0.09	0.50 ± 0.07	0.57 ± 0.06	0.56 ± 0.08
Accumulation Zone	0.79 ± 0.04	0.77 ± 0.02	0.76 ± 0.02	0.82 ± 0.03
Acc. Zone (N. of 70° N)	0.82 ± 0.04	0.75 ± 0.02	0.78 ± 0.01	0.83 ± 0.02
Acc. Zone (S. of 70° N)	0.77 ± 0.04	0.78 ± 0.03	0.75 ± 0.03	0.81 ± 0.03

TCD
8, 3733–3783, 2014

Table 4. Trends (and 95 % confidence intervals) in JJA albedo (fraction per decade) at GC-Net and K-Transect weather stations and the nearest, MOD10A1, MCD43A3, and MAR pixels. In this case, MODIS data flagged as "other quality" have been included. Only 16 day periods when coincident estimates are available for all datasets have been used. Values in bold indicate trends significant at the 95 % confidence level.

	Period	MCD43A3 BSA Shortwave	MOD10A1	MAR clear-sky	In Situ
Ablation Zone					
Swiss Camp (GC)	2000–2011	**−0.15** ± 0.05	**−0.15** ± 0.06	**−0.05** ± 0.03	**−0.06** ± 0.03
JAR 1 (GC-Net)	2000–2012	**−0.19** ± 0.06	**−0.21** ± 0.07	**−0.07** ± 0.03	**−0.22** ± 0.03
JAR 2 (GC-Net)	2000–2012	**−0.06** ± 0.02	**−0.08** ± 0.03	**−0.04** ± 0.02	< 0.01 ± 0.02
S5 (K-Transect)	2004–2012	**−0.05** ± 0.03	**−0.09** ± 0.04	−0.04 ± 0.04	**−0.08** ± 0.04
S6 (K-Transect)	2004–2012	**−0.13** ± 0.07	**−0.19** ± 0.08	**−0.08** ± 0.06	**−0.14** ± 0.06
S9 (K-Transect)	2004–2012	**−0.15** ± 0.05	**−0.17** ± 0.06	**−0.12** ± 0.05	**−0.25** ± 0.05
Accumulation Zone, North of 70° N					
Humboldt (GC)	2002–2011	−0.01 ± 0.02	**−0.05** ± 0.02	**−0.02** ± 0.01	< 0.01 ± 0.01
Summit (GC-Net)	2000–2012	**−0.02** ± 0.02	**−0.04** ± 0.02	**< 0.01** ± < 0.01	< 0.01± < 0.01
Tunu N (GC-Net)	2000–2012	**−0.03** ± 0.01	**−0.05** ± 0.02	−0.01 ± 0.01	< 0.01 ± 0.01
NASA-E (GC-Net)	2000–2011	**−0.02** ± 0.01	**−0.05** ± 0.02	< 0.01 ± 0.01	**−0.03** ± 0.01
Accumulation Zone, South of 70° N					
Dye-2 (GC-Net)	2000–2012	**−0.05** ± 0.01	**−0.07** ± 0.02	**−0.01** ± 0.01	−0.01 ± 0.01
Saddle (GC-Net)	2000–2012	**−0.03** ± 0.01	**−0.05** ± 0.02	**−0.01** ± 0.01	−0.01 ± 0.01
South Dome (GC)	2003–2012	**−0.04** ± 0.01	**−0.06** ± 0.02	−0.01 ± 0.01	**−0.08** ± 0.01
NASA SE (GC)	2000–2012	**−0.04** ± 0.01	**−0.07** ± 0.02	**−0.02** ± 0.01	< 0.01 ± 0.01

TCD
8, 3733–3783, 2014

Table 5. Mean and standard deviation for the best fit to the distributions of ablation zone albedo shown in Fig. 14 (assuming that the appropriate distribution is a combination of two normal distributions).

	MOD10A1	MCD43A3 BSA Shortwave	MAR v2.0 Cloud-Corrected	MAR v3.2 Cloud-Corrected
First Mode (Ice)	0.57 ± 0.10	0.55 ± 0.10	0.50 ± 0.05	0.61 ± 0.06
Second Mode (Snow)	0.73 ± 0.06	0.71 ± 0.04	0.74 ± 0.04	0.74 ± 0.03

TCD
8, 3733–3783, 2014

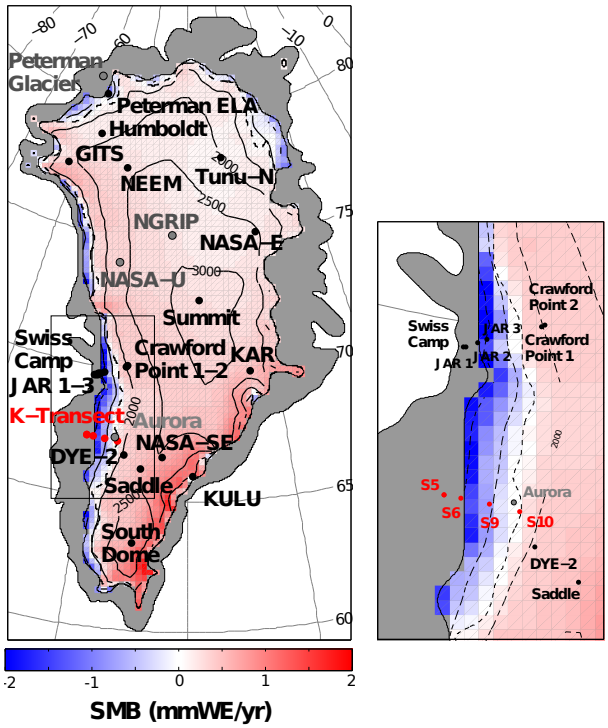

Figure 1. MAR v3.2 mean September 2000–August 2013 SMB (mWE yr^{-1}) and locations of all GC-Net and K-Transect weather stations. Pixels not defined as 100 % ice covered in MAR are masked out. The bold dotted black line shows the mean equilibrium line (where the mean SMB is 0). The K-transect stations (S5, S6, S9, S10) are colored red, while GC-Net stations are black. Stations in grey are GC-Net stations that have not been used in this study. Other contour lines indicate elevation in m a.s.l.. The inset shows individual stations near the west coast ablation zone.

TCD
8, 3733–3783, 2014

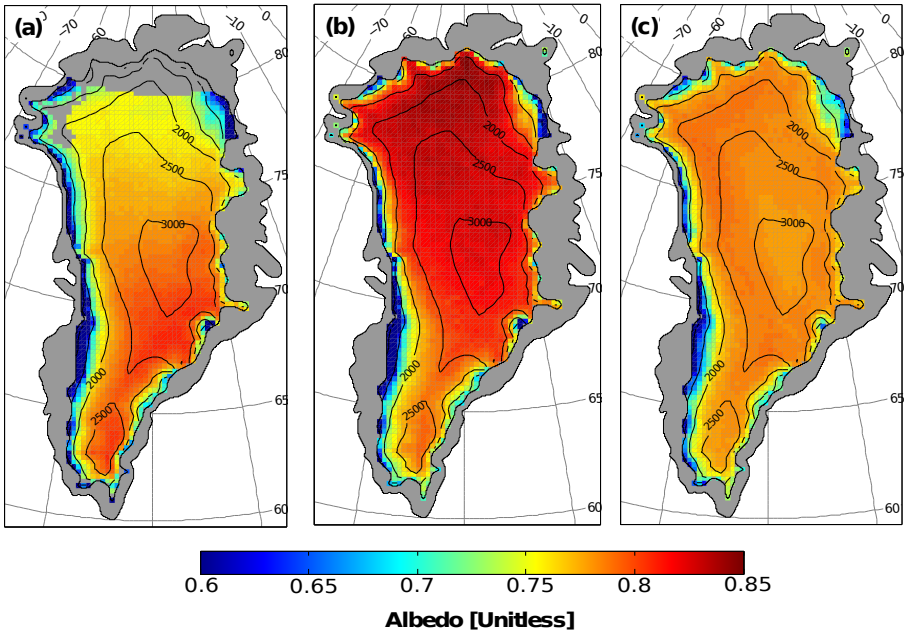

Figure 2. Mean 2000–2013 June, July, August (JJA) albedo (unitless) for **(a)** the MCD43A3 BSA shortwave product (on the MAR grid) **(b)** MOD10A1 product (on the MAR grid), and **(c)** MAR v3.2 clear-sky albedo. Only good quality data MODIS data are used here.

TCD
8, 3733–3783, 2014

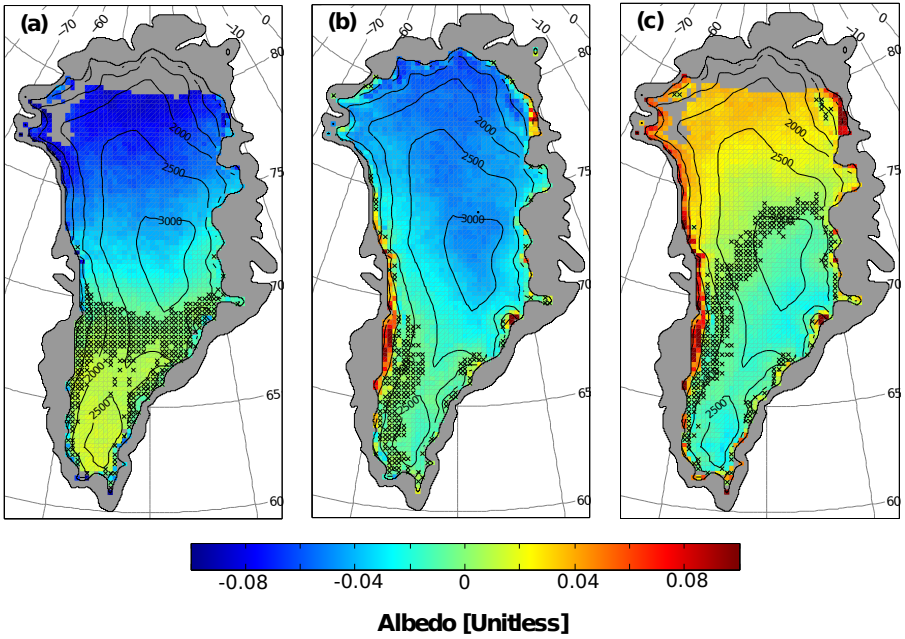

Figure 3. Mean difference in JJA albedo (unitless) for the 2000–2013 period: **(a)** MCD43A3 BSA shortwave minus MOD10A1 **(b)** MAR v3.2 clear-sky minus MOD10A1, and **(c)** MAR v3.2 clear-sky minus MCD43A3. In each case, only coincident data for each of the two datasets being compared is used.

TCD
8, 3733–3783, 2014

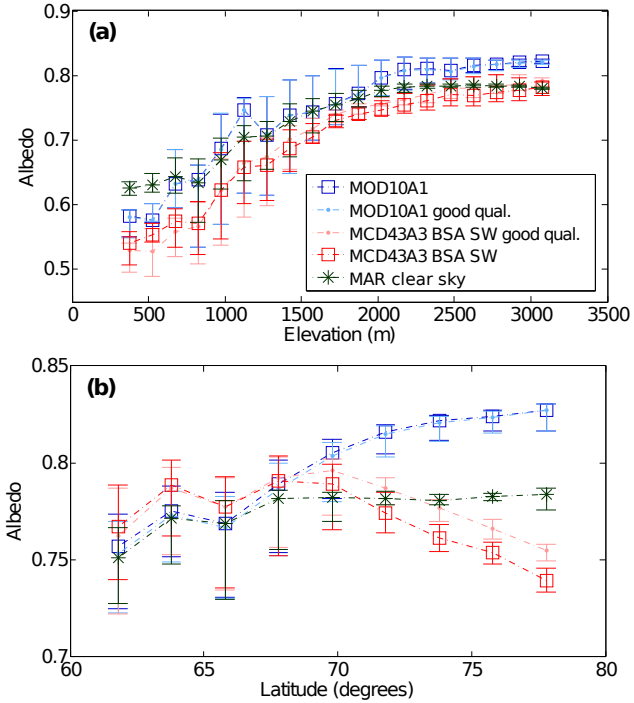

Figure 4. (a) Mean 2000–2013 JJA MOD10A1, MCD43A3 BSA shortwave (SW), and MAR v3.2 clear sky GrIS albedo (unitless) as a function of elevation divided into 150 m elevation bands. Error bars indicate standard deviation within each elevation band. **(b)** The same as **(a)** but for albedo as a function of latitude, divided into 2° Latitude bands. "Good qual." indicates results obtained by only using "good quality" MODIS data. "All qual." Indicates that all available MODIS observations have been used.

TCD
8, 3733–3783, 2014

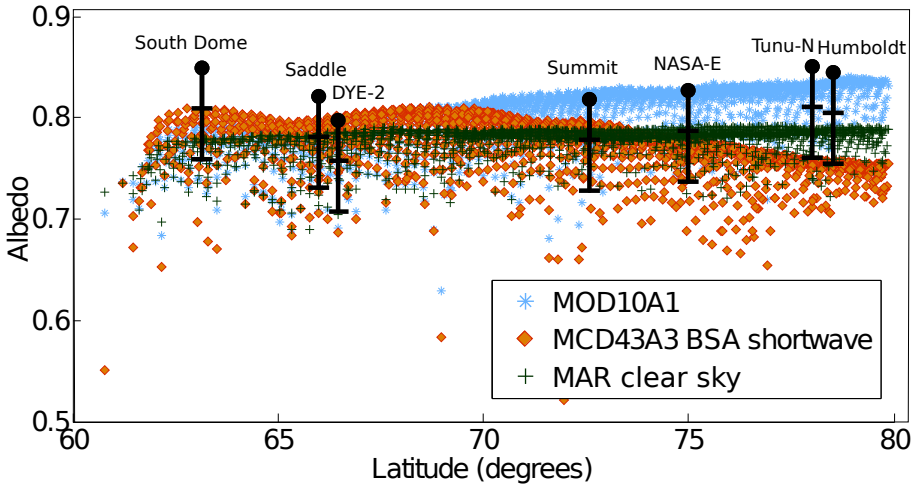

Figure 5. 2000–2012 mean JJA albedo (unitless) for the MAR accumulation zone vs. latitude, for MOD10A1, MCD43A3 BSA shortwave, MAR v3.2 clear-sky, and GC-Net station data (black circles) for stations with a record spanning at least 7 years of the 2000–2012 period. Only MODIS data flagged as "good quality" are used here. The error bars for GC-Net stations indicate the range of corrections to GC-Net data (between 0.04 and 0.09) employed by Stroeve et al. (2005).

TCD
8, 3733–3783, 2014

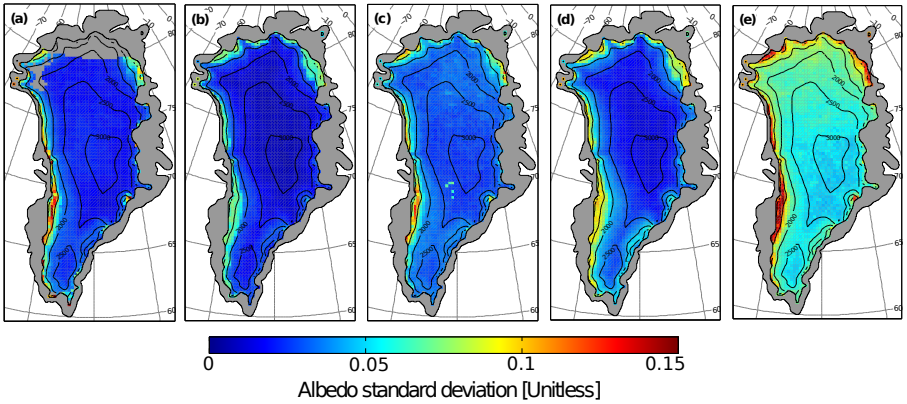

Figure 6. Standard deviation of JJA albedo (unitless) (2000–2013) for **(a)** MCD43A3 shortwave BSA **(b)** MAR v3.2 clear sky 16 day averages **(c)** MOD10A1 16 day averages **(d)** MAR v3.2 clear sky daily, and **(e)** MOD10A1 daily.

TCD
8, 3733–3783, 2014

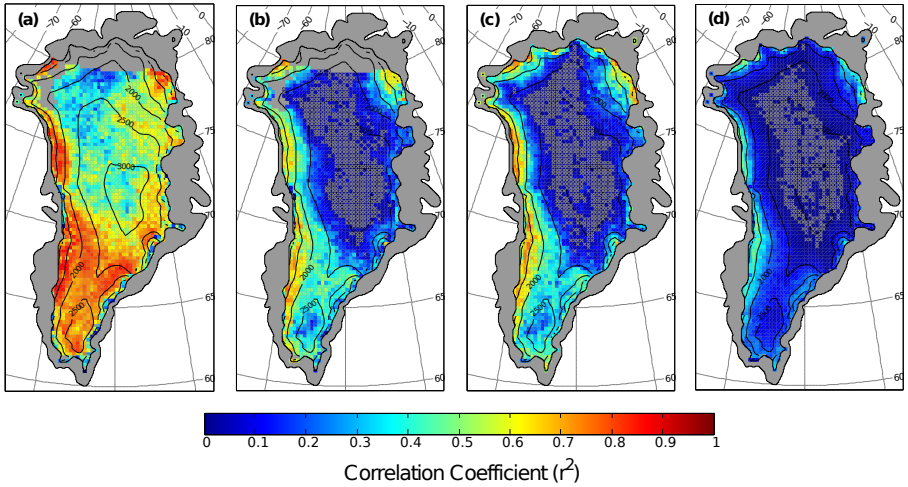

Figure 7. Correlation coefficients (r^2 values) for the 2000–2013 period during JJA for **(a)** MOD10A1 (averaged to 16 day periods) vs. MCD43A3 BSA shortwave **(b)** MAR v3.2 clear sky (16 day data) vs. MCD43A3 BSA shortwave, **(c)** MAR v3.2 clear sky (16 day data) vs. MOD10A1 (16 day data), and **(d)** MAR v3.2 clear sky (daily) vs. MOD10A1 (daily). MAR grid boxes where the correlation is not statistically significant are marked with a grey "x".

TCD
8, 3733–3783, 2014

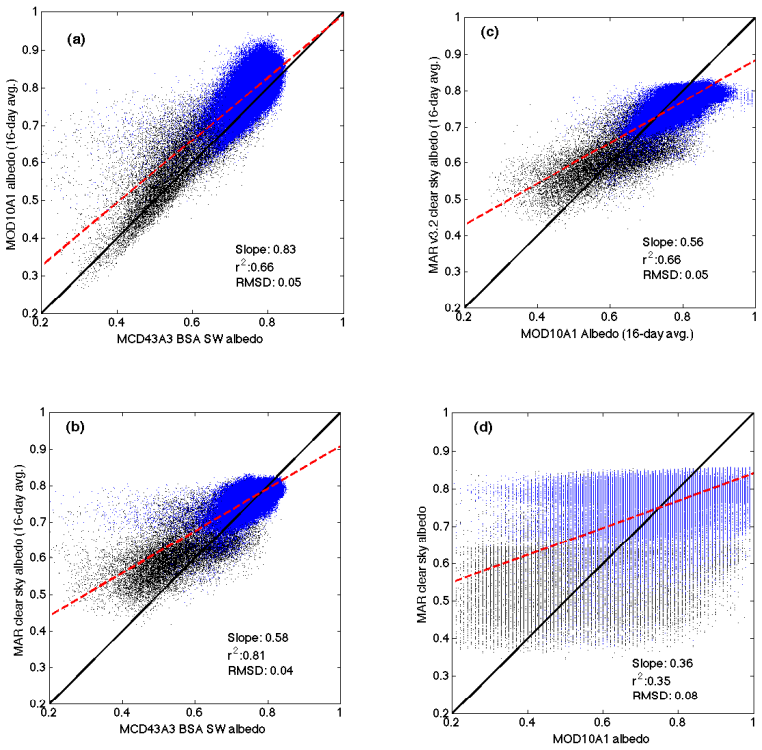

Figure 8. Scatter plots for 2000–2013 JJA albedo for **(a)** MOD10A1 (16 day averaged) vs. MCD43A3 BSA shortwave albedo (unitless) **(b)** MAR v3.2 clear-sky (16 day) vs. MCD43A3 BSA shortwave albedo, **(c)** MAR v3.2 clear-sky (16 day) vs. MOD10A1 (16 day) albedo, and **(d)** MAR v3.2 clear-sky vs. MOD10A1 (daily) albedo. Black points indicate ablation zone locations, while blue points indicate locations within the accumulation zone as defined using MAR v3.2. A solid black line indicates the 1 : 1 line, and dashed red lines indicate the best linear fit.

TCD
8, 3733–3783, 2014

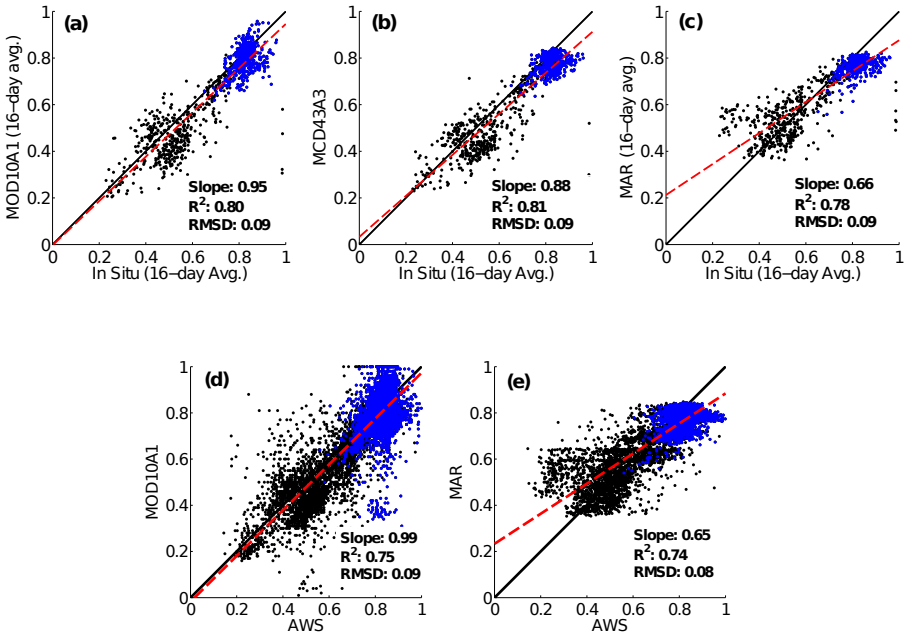

Figure 9. Scatter plots of 2000–2012 JJA mean albedo (unitless) vs. automatic weather station (GC-Net and K-Transect) albedo: **(a)** MOD10A1 16 day averages vs. 16 day in situ **(b)** MCD43A3 BSA shortwave vs. 16 day in-situ **(c)** MAR v3.2 clear sky 16 day vs. 16 day in situ **(d)** MOD10A1 vs. in situ (daily) and **(e)** MAR v3.2 vs. in situ (daily). The black lines in each figure indicate the 1 : 1 line. In this comparison, MODIS data have not been aggregated to the MAR grid. Black points indicate ablation zone locations, while blue points indicate locations within the accumulation zone as defined using MAR v3.2. Solid black lines show the 1 : 1 line, and red dashed lines indicate the best linear fit.

TCD
8, 3733–3783, 2014

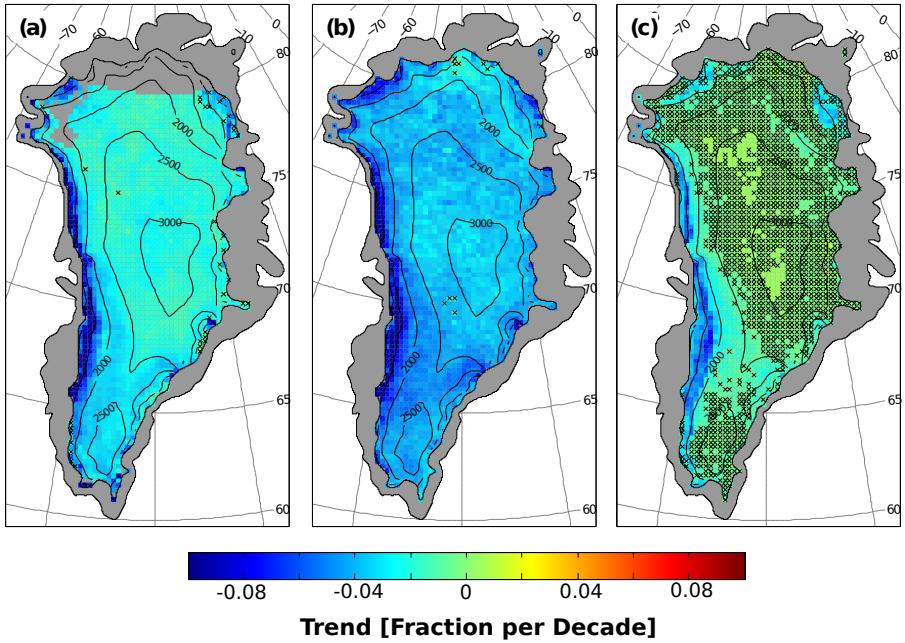

Figure 10. JJA mean albedo trends (2000–2013) in units of fraction per decade for **(a)** MCD43A3 BSA shortwave albedo, **(b)** MOD10A1 albedo, and **(c)** MAR clear-sky albedo. Grid boxes where trends are not significant at the 95 % level are marked with a black "x".

TCD
8, 3733–3783, 2014

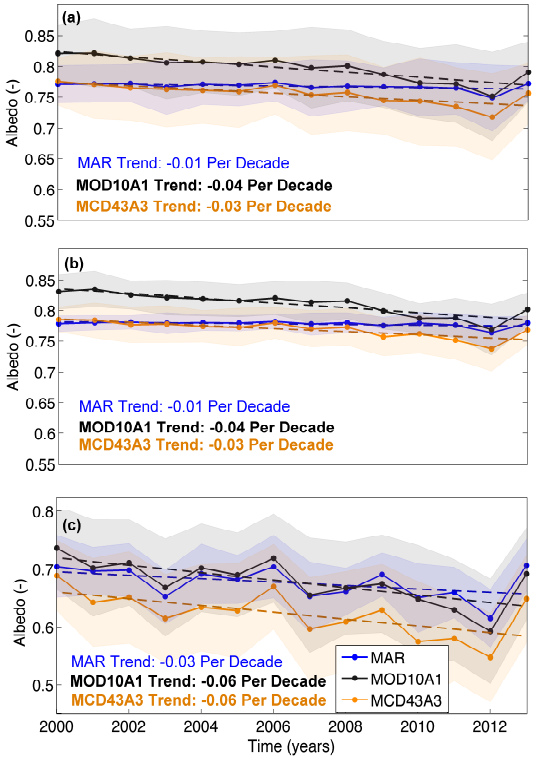

Figure 11. Mean annual JJA ice sheet albedo (solid lines) simulated by MAR v3.2 (clear-sky) (blue), MOD10A1 (black) and MCD43A3 BSA shortwave (orange) for 2000–2013 and best linear fit (dashed lines) for **(a)** the entire ice sheet, **(b)** the accumulation zone, and **(c)** the ablation zone defined using MAR v3.2 SMB. All trends produced using annual data are statistically significant at the 95 % level for the MODIS products, but are not statistically significant for MAR. Shaded areas show annual JJA standard deviation of albedo for 16 day periods from each dataset.

TCD
8, 3733–3783, 2014

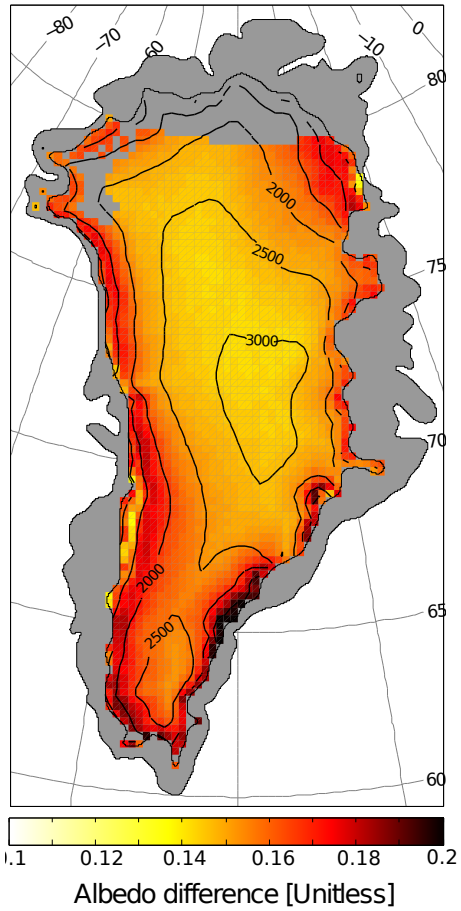

Figure 12. MCD43A3 BSA visible (0.3–0.7 µm) minus MCD43A3 BSA shortwave (0.3–5 µm) 2000–2013 JJA mean albedo (unitless) on the MAR grid. Areas not defined as 100 % ice covered in MAR v3.2 are excluded.

TCD
8, 3733–3783, 2014

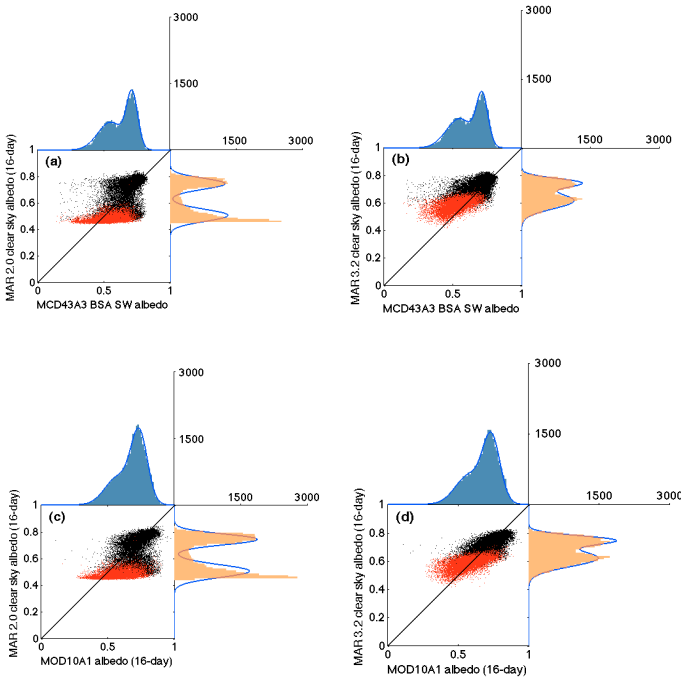

Figure 13. Scatter plots and histograms for JJA 2000–2012 albedo (unitless) within the MAR v3.2-defined GrIS ablation zone, for **(a)** MAR v2.0 clear sky (16 day avg.) vs. MCD43A3 BSA shortwave. **(b)** The same as **(a)**, but for MAR v3.2. **(c)** The same as **(a)** but for MOD10A1 albedo (averaged to 16 day periods). **(d)** The same as **(c)** but for MAR v3.2. Points where there is snow or firn (surface snowpack density > 830 kg m^{-3}) for more than 8 days of a 16 day period are shown in red. In the case of MAR v2.0, only pixels classified as 100 % ice-covered by both MAR v2.0 and v3.2 are used. Light blue curves show the best fit to each distribution obtained using maximum likelihood estimation.

TCD
8, 3733–3783, 2014

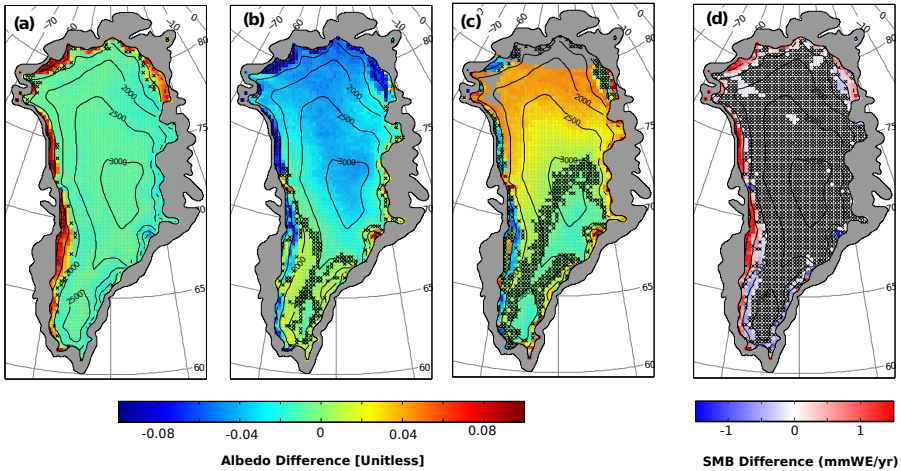

Figure 14. (a) MAR v3.2 clear-sky minus MAR v2.0 clear-sky mean JJA albedo **(b)** MAR clear-sky v2.0 minus MOD10A1 2000–2012 mean JJA albedo, **(c)** MAR clear-sky v2.0 minus MCD43A3 BSA shortwave 2000–2012 mean JJA albedo, and **(d)** MAR v3.2 minus MAR v2.0 mean JJA SMB (mWE yr^{-1}) for the same period. Grid boxes where differences are not significant at the 95 % level are marked with a black "x".

TCD
8, 3733–3783, 2014